OPEN ACCESS
IOP Publishing
Journal of Physics: Condensed Matter
J. Phys.: Condens. Matter **35** (2023) 035302 (8pp)
https://doi.org/10.1088/1361-648X/aca24f

Wannier excitons confined in hexagonal boron nitride triangular quantum dots

M F C Martins Quintela[1,2,*] **and N M R Peres**[1,2]

[1] Department of Physics and Centre of Physics of the Universities of Minho and Porto (CF–UM–UP), Campus of Gualtar, 4710-057 Braga, Portugal
[2] International Iberian Nanotechnology Laboratory (INL), Av. Mestre José Veiga, 4715-330 Braga, Portugal

E-mail: mfcmquintela@gmail.com

Received 19 September 2022, revised 25 October 2022
Accepted for publication 11 November 2022
Published 25 November 2022

Abstract

With the ever-growing interest in quantum computing, understanding the behavior of excitons in monolayer quantum dots has become a topic of great relevance. In this paper, we consider a Wannier exciton confined in a triangular quantum dot of hexagonal boron nitride. We begin by outlining the adequate basis functions to describe a particle in a triangular enclosure, analyzing their degeneracy and symmetries. Afterwards, we discuss the excitonic Hamiltonian inside the quantum dot and study the influence of the quantum dot dimensions on the excitonic states.

Keywords: hBN, quantum dot, exciton, monolayer, confined, triangular, symmetry

(Some figures may appear in colour only in the online journal)

1. Introduction

Recently, the study of monolayer quantum dots and their optical properties has gained increased traction due do their interest in quantum computing [1, 2]. The control and properties of single electrons and electron–hole pairs in qubits, the strong spin–valley coupling [3, 4], the possibility of electrically confining and manipulation of charge carriers [5], and the control of valley splitting and polarization of excitons [6], together with the possibility of optically controlling two–qubit operations in a single quantum dot [7], makes understanding excitons confined in quantum dots extremely relevant.

Further advances in understanding the triangular growth patterns of monolayer transition metal dichalcogenide (TMD) monolayers [8] led to improvements in the mechanical deposition of triangular two–dimensional TMD crystals [9]. Much more recently, methods based on the combination of periodic laser patterns, anisotropic thermal etching and endoepitaxial growth enabled the realization of monolayer nanostructures with atomically sharp interfaces [10]. The stability of triangular quantum dots has also been considered for both regular TMDs [11] and Janus materials [12], where the chalcogen layers above and below the transition metal layer are composed of different materials [13–15].

Optical, electronic and magnetic properties of TMD quantum dots are of special interest for quantum computing. Various recent works have focused on the study of these properties via different methods, namely tight–binding [16–18], density functional theory [3, 19] and continuum models [20–22]. Phase transitions to the metallic phase are also especially relevant, allowing for different charge excitation and decay pathways [23]. Recent experimental works have also shown that chemical treatment is a effective method for enhancing and modulating exciton emission in triangular TMD quantum dots [24]. Triangulenes, triangular graphene flakes with a lateral dimension of n benzene rings, have also been a recent point of focus due to their electronic and spintronic properties [25–27].

In this paper, we consider the simple system of Wannier excitons in a hexagonal boron nitride (hBN) triangular quantum dot figure 1. Using a finite basis method, we

* Author to whom any correspondence should be addressed.

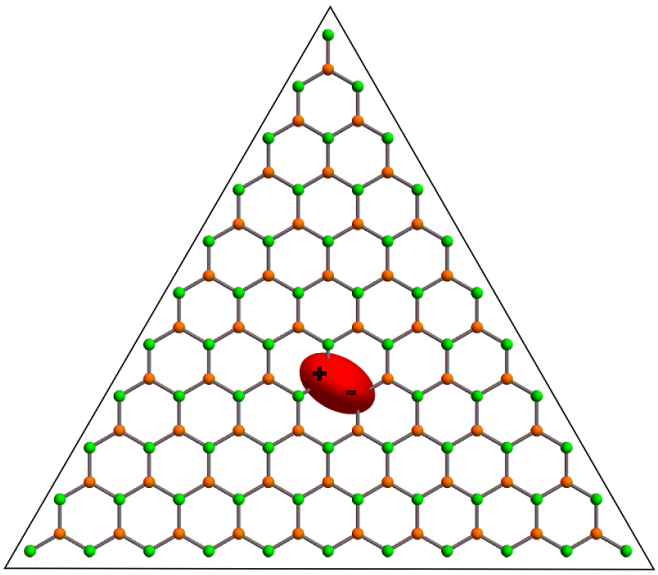

Figure 1. Schematic view of an exciton confined in a hBN triangular quantum dot with zigzag boundaries.

obtain analytical approximations to the excitonic wave functions before considering the effects of varying the size of the confinement region. This paper is structured as follows. In section 2, we begin by describing the basis of functions we will consider. This basis is created from the exact solutions for the problem of a particle in an infinite triangular well. We then perform a simple symmetry analysis of this basis such that we can more easily compute and understand the Hamiltonian for the excitonic system. In section 3, we turn our attention to the Wannier equation in a triangular quantum dot, discussing the electrostatic interaction between the electron and hole. Focusing our attention on hBN, we compute the effective masses from the band structure before studying the convergence of the method as the basis size grows. Finally, in section 4, we vary the size of the triangular quantum dot to understand the effects of confinement on each individual excitonic state.

2. Triangular quantum dots

We will first begin by considering a particle confined in an equilateral triangle with hard boundaries. The eigenvalue problem of the Schrödinger equation for an equilateral triangle with hard boundaries was solved by Lamé [28] in 1852. As in the well known case of a rectangle, this solution is a finite sum of plane waves, built to satisfy the boundary conditions. It has been proven that the only polygons that share this feature are the square, the rectangle, the equilateral triangle, the half-square (right isosceles triangle) and the half equilateral triangle ($30^\circ - 60^\circ$ triangle) [29, 30].

2.1. Analytical solution of triangular well

The solution to the particle in the triangular well has been studied through various different lenses, resulting in somewhat different expressions that all turn out to be equivalent [31–36].

We will focus our studies on the solution provided by Gaddah [36], developed for an equilateral triangle of side L with vertices A, B, C located at $(0,0)$, $(L,0)$ and $\left(L/2,\sqrt{3}L/2\right)$, respectively. The Schrödinger equation for a particle of mass μ confined in the infinite triangular well defined by the vertices A, B, C is written as

$$-\frac{\hbar^2}{2\mu}\left(\frac{\partial^2}{\partial x^2}+\frac{\partial^2}{\partial y^2}\right)\Psi(x,y)=E\Psi(x,y), \tag{1}$$

and subjected to the Dirichlet condition that $\Psi(x,y)$ vanishes on the perimeter of the triangle.

Applying a procedure based on group theory [36], the eigenfunctions are split into two different functional classes

$$\Psi^{(j)}_{n,m}(x,y)=\begin{cases} N_1\,\mathrm{Re}\left\{W(z,z^*)\right\}, & j=1\\ N_2\,\mathrm{Im}\left\{W(z,z^*)\right\}, & j=2,\end{cases} \tag{2}$$

where $z=x+iy$ and N_j are normalization constants. The function $W(z,z^*)$ can be expressed as the determinant of a 3×3 matrix as

$$W(z,z^*)=\begin{vmatrix} 1 & 1 & 1\\ e^{i\beta n(x+\sqrt{3}y)} & e^{i\beta n(x-\sqrt{3}y)} & e^{-2\,i\beta nx}\\ e^{-i\beta m(x+\sqrt{3}y)} & e^{-i\beta m(x-\sqrt{3}y)} & e^{2\,i\beta mx}\end{vmatrix}, \tag{3}$$

where $\beta=2\pi/3L$. Expanding the two different functional classes, the eigenstates are given by

$$\begin{aligned}\Psi^{(1)}_{n,m}(x,y)=2\,N_1\Big[&\sin\left(\beta\,(m-n)\,x\right)\sin\left(\sqrt{3}\beta\,(n+m)\,y\right)\\ &+\sin\left(\beta\,(n+2m)\,x\right)\sin\left(\sqrt{3}\beta ny\right)\\ &-\sin\left(\beta\,(2n+m)\,x\right)\sin\left(\sqrt{3}\beta my\right)\Big],\end{aligned} \tag{4}$$

$$\begin{aligned}\Psi^{(2)}_{n,m}(x,y)=2\,N_2\Big[&\cos\left(\beta\,(m-n)\,x\right)\sin\left(\sqrt{3}\beta\,(n+m)\,y\right)\\ &-\cos\left(\beta\,(n+2\,m)\,x\right)\sin\left(\sqrt{3}\beta ny\right)\\ &-\cos\left(\beta\,(2n+m)\,x\right)\sin\left(\sqrt{3}\beta my\right)\Big].\end{aligned} \tag{5}$$

The quantum numbers n, m obey the restriction

$$m\geqslant n>0, \tag{6}$$

with the values $m=n$ only allowed for the functions $\Psi^{(2)}_{n,m}(x,y)$ as they lead to the trivial zero solution for $\Psi^{(1)}_{n,m}(x,y)$. The orthogonality of these eigenfunctions is ensure by both Rellich's theorem [37], for eigenfunctions corresponding to distinct eigenvalues, and by direct integration of the different eigenfunctions when the eigenvalues are degenerate.

The energy eigenvalues are given by

$$E_{n,m}=\frac{8\,\pi^2\hbar^2}{9\,\mu L^2}\left(n^2+nm+m^2\right). \tag{7}$$

Since both eigenfunctions $\Psi^{(1)}_{n,m}$, $\Psi^{(2)}_{n,m}$ correspond to the same energy eigenvalue $E_{n,m}$, then it follows that all eigenvalues corresponding to $n\neq m$ are (at least), $2\times$ degenerate.

Higher order degeneracy can also occur accidentally, as well as in cases where $n = m$ (e.g. the state $\Psi^{(2)}_{n=7,m=7}$ is degenerate with the two states $\Psi^{(1)}_{n=2,m=11}$, $\Psi^{(2)}_{n=2,m=11}$).

2.2. Symmetry analysis of truncated basis

In order to truncate the eigenfunction basis, we will need to sort them in some way. To do this in a reasonable manner, we will sort the eigenfunctions by increasing energy eigenvalue. This can be easily done, as the set of all acceptable values of n, m can be expressed as

$$m = n + s, \qquad n = 1, 2, 3, ..., \tag{8}$$

with $s \in \{1, 2, 3, \ldots\}$ for $\Psi^{(1)}_{n,m}(x,y)$ and $s \in \{0, 1, 2, 3, \ldots\}$ for $\Psi^{(2)}_{n,m}(x,y)$, allowing us to quickly run through many basis functions in an algorithmic way.

From a group symmetry perspective, each $\Psi^{(1)}_{n,m}(x,y)$, $\Psi^{(2)}_{n,m}$, (x,y) eigenstate will have certain symmetries that will allow us to diagonalize the Hamiltonian in blocks, greatly speeding up the computation time and reducing the number of trivially–zero matrix elements that are computed to zero. These eigenstates are, however, not written in the usual irreducible representations of the C_{3v} point group, so a more careful analysis is required. By careful inspection of the eigenfunctions of the infinite triangular well, four different and orthogonal groupings of functions can be observed. For this discussion, we define non–negative integer k to better distinguish the functions. Firstly, the fully symmetric states are all those written as

$$\Psi^{(2)}_{n,n+3k}(x,y). \tag{9}$$

Secondly, the remaining $\Psi^{(2)}_{n,n+s}(x,y)$ (i.e. those where s mod $3 = 1$ or 2) all belong to a separate grouping in which all functions are even under reflection by the axis that crosses both the origin and the center of the triangle $\left(\frac{L}{2}, \frac{L}{2\sqrt{3}}\right)$. Thirdly, all eigenstates written as

$$\Psi^{(1)}_{n,n+3k}(x,y) \tag{10}$$

are even under rotations of $\pm 2\pi/3$ along the vertical axis that passes through the geometric center of the triangle. Fourthly and finally, the remaining $\Psi^{(1)}_{n,n+s}(x,y)$ (i.e. those where s mod $3 = 1$ or 2) are all odd under reflections by the axis that crosses both the origin and the center of the triangle. This separation matches what would be expected from the energy degeneracy of the states $\Psi^{(1/2)}_{n,m}(x,y)$, as these belong to orthogonal sets of functions.

With this block diagonalization of the Hamiltonian, we can now move to studying to convergence of this method. To do this, however, we will first introduce a notation for the states mentioned previously as to make the discussion easier to follow. The fully symmetric states will be labeled as

$$\phi_{\mathrm{Id}}(x,y),$$

the states even/odd under reflection by the axis that crosses both the origin and the center of the triangle are labeled as

$$\phi_{\pm\sigma}(x,y),$$

respectively, and the states even under rotations of $\pm 2\pi/3$ along the vertical axis that passes through the geometric center of the triangle are labeled as

$$\phi_{C_3}(x,y).$$

The quantum numbers n, s have been discarded in this section for two specific reasons. Firstly, to improve readability and clarity when discussing the states and the convergence of the method; secondly, because the functions in each orthogonal grouping will be sorted by their energies for the implementation of the method, effectively removing the meaning of each individual quantum number.

3. Wannier equation in a quantum dot

Following from the Schrödinger in a triangular well in equation (1), we will now consider the Wannier equation inside a hBN triangular dot, given by

$$-\frac{\hbar^2\nabla^2}{2\mu_{\mathrm{exc}}}\psi_\nu(\mathbf{r}) + V(\mathbf{r})\psi_\nu(\mathbf{r}) = E_{\mathrm{bind},\nu}\psi_\nu(\mathbf{r}), \tag{11}$$

where ∇^2 is the Laplacian operator, μ_{exc} is the exciton reduced mass, $\psi_\nu(\mathbf{r})$ the wave function for the excitonic state ν, $E_{\mathrm{bind},\nu} = E_\nu - E_{\mathrm{gap}}$ the binding energy associated with the excitonic state $\psi_\nu(\mathbf{r})$, with E_ν the energy of the state and E_{gap} the bandgap of the system, and $V(\mathbf{r})$ an electrostatic potential coupling the electron and the hole pair.

To obtain the excitonic binding energies and wave functions, we expand $\psi_\nu(\mathbf{r})$ in terms of the solutions of the infinite well defined in equations (4) and (5). As the electrostatic potential coupling the electron and hole pair only depends on the distance to the center of the triangular dot, the excitonic wave functions will have the same symmetry as the states $\phi_{\mathrm{Id}}, \phi_{\pm\sigma}, \phi_{\mathrm{C}_3}$. This means that equation (11) can also be diagonalized by blocks for the basis size chosen and, therefore, the wave functions can be explicitly separated by their symmetries and written as

$$\psi_{\nu,S}(\mathbf{r}) = \sum_{n=0}^{N} c_{n,S}\,\phi_{n,S}(\mathbf{r}), \tag{12}$$

where N is the basis size chosen, $\{c_n\}$ are a set of numerical coefficients yet to be determined, and $S = \{\mathrm{Id}, +\sigma, -\sigma, \mathrm{C}_3\}$ represents the symmetry of the excitonic state following the analysis from section 2.2.

To compute the reduced exciton mass μ_{exc}, we start from the low–energy Hamiltonian, given by

$$\mathcal{H}(\mathbf{k}) = \frac{E_g}{2}\sigma_z + \hbar v_F(\tau k_x\sigma_x + k_y\sigma_y), \tag{13}$$

where $2E_g = 7.8\,\text{eV}$ is the bandgap, σ_i are the Pauli matrices, $\tau = \pm 1$ is the valley index and v_F is the Fermi velocity. The band structure near the Dirac point is given by

$$E_\pm(\mathbf{k}) = \pm\sqrt{\frac{E_g^2}{4} + \hbar^2 v_F^2 k^2}, \tag{14}$$

near $k = 0$, where $\pm$ denotes the conduction/valence bands. The reduced mass of excitons in this material can be obtained from the coefficient of the quadratic term of the series expansion of the band structure present in equation (14) near $k = 0$ [38]. Performing this expansion, the relevant coefficient is given by

$$\begin{aligned}\frac{\hbar^2}{m_\pm} &= \left.\frac{\partial^2 E_\pm(\mathbf{k})}{\partial k^2}\right|_{k=0} \\ &= \pm\frac{2\,\hbar^2 v_F^2}{E_g}.\end{aligned} \tag{15}$$

The reduced exciton mass is then obtained as $\mu_{\text{exc}}^{-1} = m_+^{-1} - m_-^{-1}$, meaning that

$$\mu_{\text{exc}} = \frac{E_g}{4\,v_F^2} = 0.172 m_e, \tag{16}$$

with m_e the bare electron mass.

3.1. Electrostatic potential in layered materials

For two dimensional layered materials, the electrostatic coupling between the electron and the hole of the exciton is well–modeled [39] by the Rytova–Keldysh potential [40, 41], given by

$$V(\mathbf{r}) = -\frac{\hbar c \alpha \pi}{2 r_0}\left[H_0\left(\epsilon_r \frac{r}{r_0}\right) - Y_0\left(\epsilon_r \frac{r}{r_0}\right)\right], \tag{17}$$

where r is the in–plane position, ϵ_r is the mean dielectric constant of the medium above/below the layered material, c is the speed of light, α is the fine–structure constant, and $H_0(x)$ and $Y_0(x)$ are the Struve function and Bessel function of the second kind, respectively. The parameter r_0 corresponds to an in–plane screening length related to the 2D polarizability of the material, usually obtained via DFT [42].

Considering again our triangular dot, the hard wall confinement leads to a Dirichlet boundary condition on $\psi_\nu(\mathbf{r}) = 0$, meaning that the basis of functions defined in equations (4) and (5) is an appropriate choice for a finite basis approach. Additionally, we shift the Rytova–Keldysh potential as to be centered at the geometric center of our triangular dot, meaning that the electrostatic potential inside it now reads

$$V(\mathbf{r}) = -\frac{\hbar c \alpha \pi}{2\,r_0}\left[H_0\left(\epsilon_r \frac{r'}{r_0}\right) - Y_0\left(\epsilon_r \frac{r'}{r_0}\right)\right], \tag{18}$$

with $r' = |r - r_c| = \sqrt{(x-x_0)^2 + (y-y_0)^2}$ the distance between a point $r = (x, y)$ and the center of the triangle $r_c = (x_0, y_0)$. For freely suspended hBN, the screening length parameter in the Rytova–Keldysh potential is $r_0 = 10$ Å [43] and $\epsilon_r = 1$.

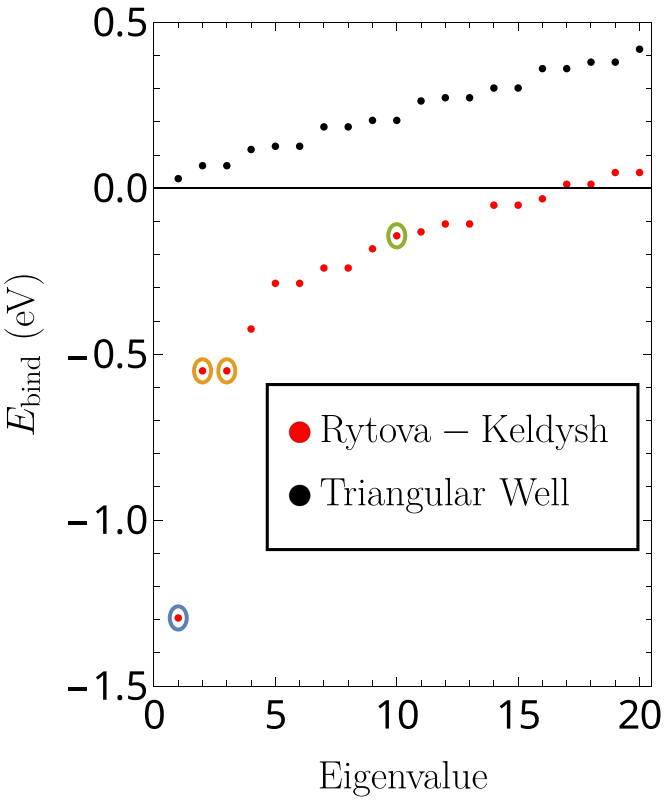

Figure 2. Spectrum of a particle confined in an infinite triangular well (black dots) and of a Wannier exciton confined to a triangular quantum dot (red dots) for a basis size of $N = 80$ and a side length $L = 200$ Å. Colored circles mark the lowest energy states from ϕ_{Id} (blue), $\phi_{\pm\sigma}$ (orange) and ϕ_{C_3} (green).

3.2. Convergence analysis

Having defined both the electrostatic potential and the reduced exciton mass in the system, we can proceed to compute the four distinct Hamiltonian blocks for each of the orthogonal representations for a specific basis size N and a specific side length L. Doing this, we compare the full low energy spectrum of the exciton confined in a triangular dot to that of the simple particle inside a triangular box in figure 2.

Focusing on the lowest energy state, belonging, as expected, to the ϕ_{Id} set of functions, we study the evolution of its energy eigenvalue as the basis size increases. In figure 3, we plot this evolution as a function of the inverse of the basis size for a triangle side length of $L = 200$ Å. We obtain the expected limiting value for the complete basis by the intersection of the fitting line with the axis as $E_{\phi_{\text{Id}}} = -1.323\,\text{eV}$.

4. Quantum dot size effects

To finalize this paper, we will now discuss the effect on the excitonic states of varying the size of the quantum dot. This is done by setting the basis size to a fixed value, in this case $N = 80$ as to greatly speed up the computation versus $N = 100$, and varying the side length of the triangular dot. To study this dependence, we plot the energy of the excitonic ground state as

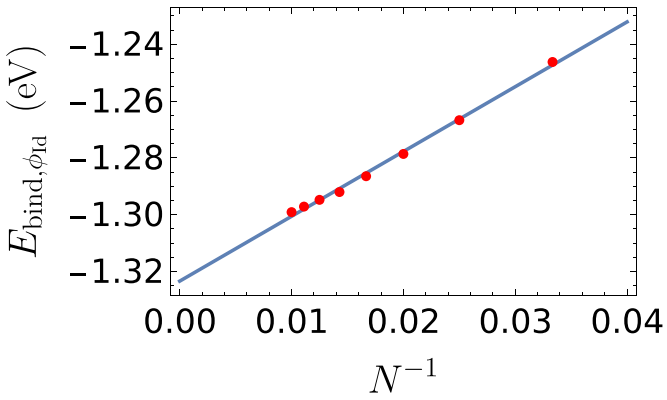

Figure 3. Scaling of the binding energy of the lowest ϕ_{Id} state as a function of $1/N$, with $N \in [30, 100]$, for $L = 200$ Å. The interception of the fitting straight–line with energy axis gives a ground state energy $E_{\phi_{\text{Id}}} = -1.323\,\text{eV}$.

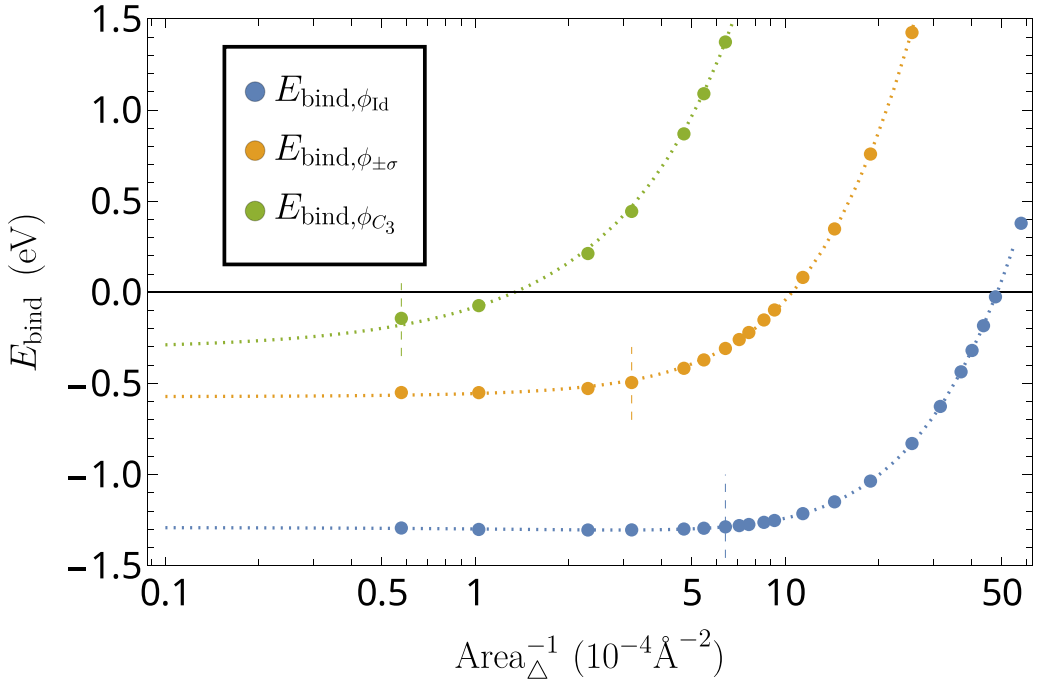

Figure 4. Scaling of the binding energy of the lowest ϕ_{Id}, $\phi_{\pm\sigma}$ and ϕ_{C_3} states as a function of the inverse of the area of the triangular dot for a side length range $L \in [20, 200]$ Å. Vertical ticks mark the area for which the specific state begins to feel confinement.

a function of the inverse of the area $\left(= \frac{\sqrt{3}L^2}{4}\right)$ of the triangular dot in figure 4. We choose this scaling as it is the same relation as that between the energy of a particle in the textbook problem of hard wall confinement in a polygonal box with hard wall confinement and the dimensions of said box (i.e. the energy of a state will be inversely proportional to the area of the box). To aid visualization, the states in question have also been marked in figure 2 with their respective colors. The wave functions of these states are also plotted in figure 5.

As the confinement effects of the triangular dot start dominating the excitonic states as the dot size shrinks, we expect a linear trend in the ground state energy as we reduced the size of the triangle. As the dot size grows, however, we expect the energy to settle to an almost constant value, as for a sufficiently large quantum dot no effects from the boundaries are felt. This is displayed in the vertical tick marks present in figure 4 marking the points at which the confinement effects become noticeable. For the excitonic ground state and first excited state, this happens at $L \approx 60$ Å and $L \approx 85$ Å, respectively. For the first state belonging to the ϕ_{C_3} block, this occurs at a side length superior to $L \approx 200$ Å. This is as expected, as the lowest energy state from the ϕ_{C_3} block is the sixth excited state in the total Hamiltonian, as is clear from figure 2.

A relevant comparison for the various side lengths is against the distance between edge atoms in the triangular dot. Considering a zigzag boundary, where the edges of the dot are all composed of the same atomic site (boron or nitrogen), the distance between two atoms in the edge is given by

$$d = 2a\cos 30^\circ = 4.347\,\text{Å}, \tag{19}$$

where $a = 2.510$ Å is the lattice parameter of hBN. As such, an edge with length L will have L/d atoms on the edge.

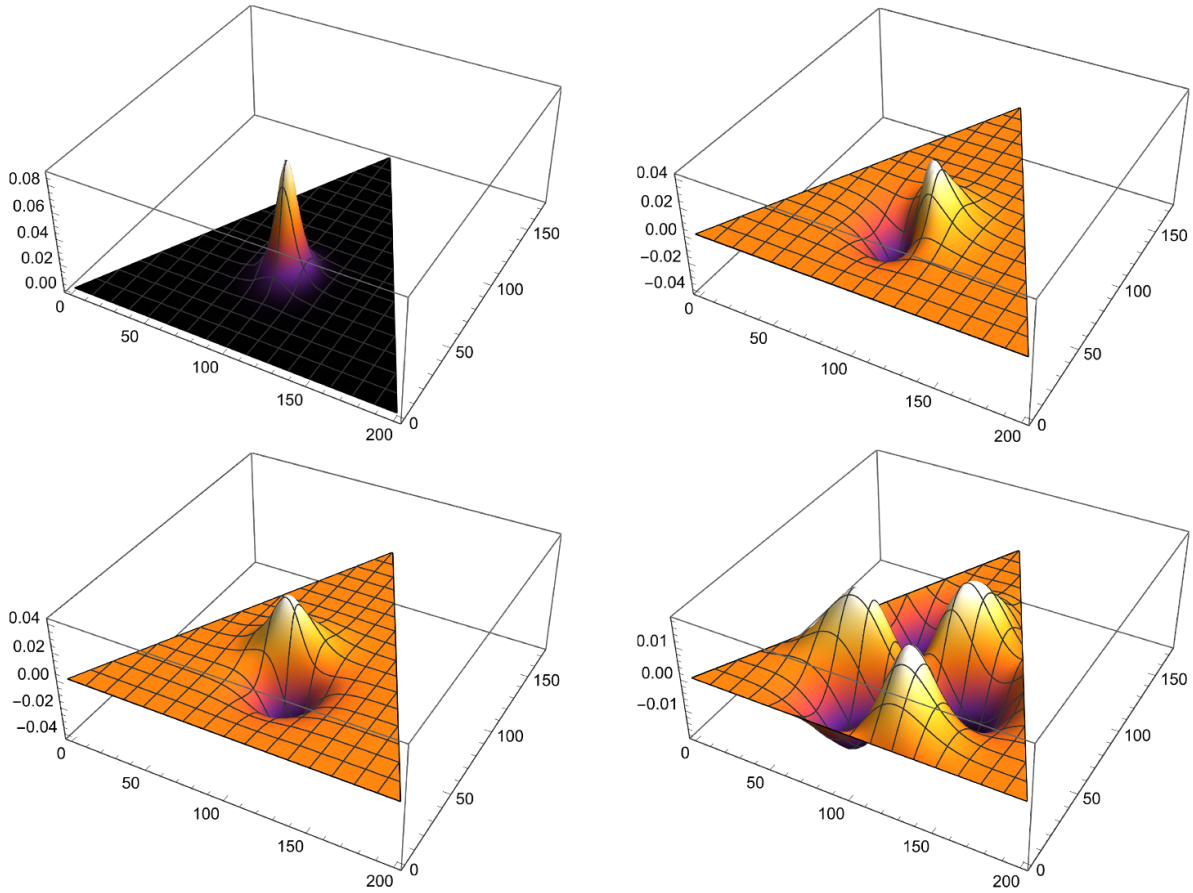

Figure 5. 3D plot of the lowest energy excitonic wave functions belonging to ϕ_{Id} (top-left), $\phi_{+\sigma}$ (top-right), $\phi_{-\sigma}$ (bottom-left), and ϕ_{C_3} (bottom-right) confined in a hBN triangular quantum dot of side $L = 200$ Å considering a basis size $N = 80$.

Finally, we will now consider both the ground state and the two times degenerate first excited state. As these three $(1+2)$ states are analogous to the $1s$ and $2p_{\pm}$ states in the 2D Hydrogen atom, we expect them to correspond to the dominant resonance in the excitonic polarizability [42, 44–46], easily accessible via pump–probe experiments [47, 48]. The ground state begins to feel the effects of the triangular confinement at $L \approx 60$ Å, which corresponds to a hBN triangular dot whose sides consist of roughly 14 atoms. The first excited state only feels the confinement effects at $L \approx 85$ Å, corresponding to an edge of roughly 20 atoms. This creates a range of side lengths in which the excitonic ground state already considers the system infinite, but the first excited states are still feeling the effects of the triangular confinement. For the quantum dot scale mentioned in reference [24] of roughly $L \approx 20\,\mu$m, already three orders of magnitude larger than the largest we have considered ($L \approx 200$ Å), we would obtain results indistinguishable from that of an infinite hBN sheet. However, the larger triangular crystals reported in reference [24] are a direct consequence of the growing crystal–formation time. Presumably, this growing time can be reduced leading to smaller triangular crystals.

5. Conclusions

In this paper, we have studied the properties of excitons confined to triangular quantum dots. We began by discussing an appropriate basis of functions to obtain an approximate solution to the Wannier equations. These functions follow from the solution of the Schrödinger equation for a particle confined to a triangular well, where analytical closed form solutions are well known. Afterwards, we briefly analyzed the symmetry of these wave functions so that we could more efficiently compute the energy expectation values and, therefore, reduce the computational time. This symmetry analysis provides valuable information about the degeneracy of each excitonic state, as well as understanding which dipolar transitions one can expect to be allowed.

Afterwards, we considered Wannier excitons confined in a hBN quantum dot, explicitly writing the electrostatic coupling between electron and hole as well as their respective reduced masses. The convergence of the method with increasing basis size was also discussed.

Finally, we considered the effects of decreasing the size of the quantum dot on the excitonic states. As expected, the more

energetic states are more sensible to confinement as they are more spread out over the dot. We focused our attention on the two lowest energy states, analogous to the Hydrogen 1 *s* and 2 *p* states, as transitions between these are expected to dominate the excitonic linear polarizability.

Data availability statement

All data that support the findings of this study are included within the article (and any supplementary files).

Acknowledgments

M F C M Q acknowledges the International Iberian Nanotechnology Laboratory (INL) and the Portuguese Foundation for Science and Technology (FCT) for the Quantum Portugal Initiative (QPI) Grant SFRH/BD/151114/2021.

N M R P acknowledges support by the Portuguese Foundation for Science and Technology (FCT) in the framework of the Strategic Funding UIDB/04650/2020, COMPETE 2020, PORTUGAL 2020, FEDER, and FCT through Projects PTDC/FIS-MAC/2045/2021, EXPL/FIS-MAC/0953/2021, and from the European Commission through the project Graphene Driven Revolutions in ICT and Beyond (Reference No. 881603, CORE 3).

ORCID iDs

M F C Martins Quintela https://orcid.org/0000-0002-0961-9235
N M R Peres https://orcid.org/0000-0002-7928-8005

References

[1] Krenner H J, Stufler S, Sabathil M, Clark E C, Ester P, Bichler M, Abstreiter G, Finley J J and Zrenner A 2005 Recent advances in exciton-based quantum information processing in quantum dot nanostructures *New J. Phys.* **7** 184
[2] Maragkou M 2015 The dark exciton as a qubit *Nat. Mater.* **14** 260
[3] Kormányos A, Zólyomi V, Drummond N D and Burkard G 2014 Spin–orbit coupling, quantum dots and qubits in monolayer transition metal dichalcogenides *Phys. Rev.* X **4** 011034
[4] Mak K F, Xiao D and Shan J 2018 Light–valley interactions in 2D semiconductors *Nat. Photon.* **12** 451–60
[5] Wang K *et al* 2018 Electrical control of charged carriers and excitons in atomically thin materials *Nat. Nanotechnol.* **13** 128–32
[6] Qu F, H Bragança, Vasconcelos R, Liu F, Xie S-J and Zeng H 2019 Controlling valley splitting and polarization of dark- and bi-excitons in monolayer WS_2 a tilted magnetic field *2D Mater.* **6** 045014
[7] Wu Y, Tong Q, Liu G-B, Yu H and Yao W 2016 Spin-valley qubit in nanostructures of monolayer semiconductors: optical control and hyperfine interaction *Phys. Rev.* B **93** 045313
[8] Zhu S and Wang Q 2015 A simple method for understanding the triangular growth patterns of transition metal dichalcogenide sheets *AIP Adv.* **5** 107105
[9] Rajan A G, Warner J H, Blankschtein D and Strano M S 2016 Generalized mechanistic model for the chemical vapor deposition of 2D transition metal dichalcogenide monolayers *ACS Nano* **10** 4330–44
[10] Liu C and Liu K 2022 Monolayer mosaic heterostructures *Nat. Nanotechnol.* **17** 439–40
[11] Dhenadhayalan N, Lin T-W, Lee H-L and Lin K-C 2018 Multisensing capability of $MoSe_2$ quantum dots by tuning surface functional groups *ACS Appl. Nano Mater.* **1** 3453–63
[12] Paez-Ornelas J I, Ponce-Pérez R, Fernández-Escamilla H N, Hoat D M, Murillo-Bracamontes E A, Moreno-Armenta Mia G, Galván D H and Guerrero-Sánchez J 2021 The effect of shape and size in the stability of triangular Janus MoSSe quantum dots *Sci. Rep.* **11** 21061
[13] Lu A-Y *et al* 2017 Janus monolayers of transition metal dichalcogenides *Nat. Nanotechnol.* **12** 744–9
[14] Zhang J *et al* 2017 Janus monolayer transition-metal dichalcogenides *ACS Nano* **11** 8192–8
[15] Yagmurcukardes M, Qin Y, Ozen S, Sayyad M, Peeters F M, Tongay S and Sahin H 2020 Quantum properties and applications of 2D Janus crystals and their superlattices *Appl. Phys. Rev.* **7** 011311
[16] Ávalos-Ovando O, Mastrogiuseppe D and Ulloa S E 2016 Noncollinear exchange interaction in transition metal dichalcogenide edges *Phys. Rev.* B **93** 161404
[17] Ávalos-Ovando O, Mastrogiuseppe D and Ulloa S E 2016 Symmetries and hybridization in the indirect interaction between magnetic moments in MoS_2d nanoflakes *Phys. Rev.* B **94** 245429
[18] Ávalos-Ovando O, Mastrogiuseppe D and Ulloa S E 2018 Long range of indirect exchange interaction on the edges of MoS_2 flakes *J. Phys.: Condens. Matter* **30** 045801
[19] Tiutiunnyk A *et al* 2022 Electronic, optical and magnetic properties of doped triangular MoS_2 quantum dots: a density functional theory approach *Phys. Status Solidi* b **259** 2100509
[20] Ezawa M 2010 Dirac fermions in a graphene nanodisk and a graphene corner: texture of vortices with an unusual winding number *Phys. Rev.* B **81** 201402
[21] Li L L, Zarenia M, Xu W, Dong H M and Peeters F M 2017 Exciton states in a circular graphene quantum dot: magnetic field induced intravalley to intervalley transition *Phys. Rev.* B **95** 045409
[22] Mittelstädt A, Schliwa A and Klenovský P 2022 Modeling electronic and optical properties of III–V quantum dots—selected recent developments *Light Sci. Appl.* **11** 17
[23] Kim B-H, Jang M-H, Yoon H, Kim H J, Cho Y-H, Jeon S and Song S-H 2021 Metallic phase transition metal dichalcogenide quantum dots showing different optical charge excitation and decay pathways *NPG Asia Mater.* **13** 41
[24] Dhakal K P, Roy S, Yun S J, Ghimire G, Seo C and Kim J 2017 Heterogeneous modulation of exciton emission in triangular WS_2 monolayers by chemical treatment *J. Mater. Chem.* C **5** 6820–7
[25] Su J *et al* 2019 Atomically precise bottom-up synthesis of π-extended [5]triangulene *Sci. Adv.* **5** eaav7717
[26] Hieulle J *et al* 2021 On-surface synthesis and collective spin excitations of a triangulene-based nanostar *Angew. Chem., Int. Ed. Engl.* **60** 25224–9
[27] Ortiz R, Catarina G and Fernández-Rossier J 2022 Theory of triangulene two-dimensional crystals (arXiv:2206.14907)
[28] Lamé G 1852 *Leçons sur la ThéOrie MathéMatique de l'Elasticité* (Paris: Bachelier)
[29] Amar V, Pauri M and Scotti A 1991 Schrödinger-equation for convex plane polygons—a tiling method for the

derivation of eigenvalues and eigenfunctions *J. Math. Phys.* **32** 2442–9
[30] Amar V, Pauri M and Scotti A 1993 Schrödinger-equation for convex plane polygons .2. A no-go theorem for plane-waves representation of solutions *J. Math. Phys.* **34** 3343–50
[31] Richens P J and Berry M V 1981 Pseudointegrable systems in classical and quantum mechanics *Physica* D **2** 495–512
[32] Krishnamurthy H R, Mani H S and Verma H C 1982 Exact solution of the Schrodinger equation for a particle in a tetrahedral box *J. Phys. A: Math. Gen.* **15** 2131–7
[33] Turner J W 1984 On the quantum particle in a polyhedral box *J. Phys. A: Math. Gen.* **17** 2791–7
[34] Li W-K and Blinder S M 1985 Solution of the Schrödinger equation for a particle in an equilateral triangle *J. Math. Phys.* **26** 2784–6
[35] McCartin B J 2003 Eigenstructure of the equilateral triangle, part I: the dirichlet problem *SIAM Rev.* **45** 267–87
[36] Gaddah W 2013 A lie group approach to the Schrödinger equation for a particle in an equilateral triangular infinite well *Eur. J. Phys.* **34** 1175–86
[37] MacCluer C R 1994 *Boundary Value Problems And Orthogonal Expansions* (Piscataway, NJ: IEEE Press)
[38] Martins Quintela M F C, Henriques J C G, Tenório L G M and Peres N M R 2022 Theoretical methods for excitonic physics in 2D materials *Phys. Status Solidi* b **259** 2200097
[39] Trolle M L, Pedersen T G and Véniard V 2017 Model dielectric function for 2D semiconductors including substrate screening *Sci. Rep.* **7** 39844
[40] Rytova S N 1967 The screened potential of a point charge in a thin film *Mosc. Univ. Phys. Bul.* **22** 30–37
[41] Keldysh L V 1979 Coulomb interaction in thin semiconductor and semimetal films *Sov. J. Exp. Theor. Phys. Lett.* **29** 658
[42] Tian T, Scullion D, Hughes D, Li L H, Shih C-J, Coleman J, Chhowalla M and Santos E J G 2020 Electronic polarizability as the fundamental variable in the dielectric properties of two-dimensional materials *Nano Lett.* **20** 841
[43] Henriques J C G, Ventura G B, Fernandes C D M and Peres N M R 2020 Optical absorption of single-layer hexagonal boron nitride in the ultraviolet *J. Phys.: Condens. Matter* **32** 025304
[44] Fröhlich D, Nöthe A and Reimann K 1985 Observation of the resonant optical stark effect in a semiconductor *Phys. Rev. Lett.* **55** 1335–7
[45] Berghäuser G, Knorr A and Malic E 2016 Optical fingerprint of dark 2p-states in transition metal dichalcogenides *2D Mater.* **4** 015029
[46] Berghäuser G, Steinleitner P, Merkl P, Huber R, Knorr A and Malic E 2018 Mapping of the dark exciton landscape in transition metal dichalcogenides *Phys. Rev.* B **98** 020301
[47] Poellmann C, Steinleitner P, Leierseder U, Nagler P, Plechinger G, Porer M, Bratschitsch R, Schüller C, Korn T and Huber R 2015 Resonant internal quantum transitions and femtosecond radiative decay of excitons in monolayer WSe_2 *Nat. Mater.* **14** 889–93
[48] Merkl P *et al* 2019 Ultrafast transition between exciton phases in van der waals heterostructures *Nat. Mater.* **18** 691–6